Two-Dimensional Analysis of End Effects in Diagonal Type Nonequilibrium Plasma MHD Generator

By

Motoo ISHIKAWA* and Jūrō UMOTO**

(Received June 30, 1976)

Abstract

In this paper the authors investigate two-dimensionally the influences of the arrangement of the output electrodes and the attenuation of the magnetic induction on the current distribution etc. in the end regions of the diagonal type nonequilibrium plasma MHD generator. As a main result, it is made clear that the eddy current in the ends of the generator can be almost nullified by a proper distribution of the magnetic induction and a suitable arrangement of the output electrodes, that the variety of the dispositions of the output electrodes has little influence on the current distribution etc.

1. Introduction

In a nonequilibrium plasma MHD generator, we can use the working gas of a lower temperature and also hope to raise the efficiency, power density etc. in comparison with a combustion gas plasma MHD generator.

Next, the diagonal type generator can be operated with a single load. Hence, it needs only one DC-AC converter. Therefore, the transmission system, control system etc. containing the generator are more simplified than those containing the Faraday type generator which is operated with multi-loads.

Since near the entrance and exit of the generator there inevitably exist regions suffering spatial variation of magnetic flux density or induction intensity, and since the working gas has an electrical conductivity, the spatial differences of induced electromotive forces are created in the direction of the field attenuation. As a consequence, an eddy current occurs there. The eddy current distorts the current distribution in the generator duct end and degrades the efficiency, output power etc. of the generator. In addition, since the diagonal type generator has the output electrodes at the entrance and exit, the end effects in the diagonal type generator should be investigated in detail.

* Institute of Atomic Energy
** Department of Electrical Engineering

However, up to now these end effects have been little investigated, while those in the Faraday type generator have been already discussed in detail by Hurwitz, Dzung, Noriss, Houben et al.[1),2),3),4)].

Accordingly, in this paper the authors study two-dimensionally on the influences of the arrangement of the output electrodes and the attenuation of the magnetic induction along the generator duct on the current and potential distributions etc. near the entrance and exit of the diagonal type nonequilibrium plasma MHD generator[5)].

2. Basic Equations

2.1 Basic equations

In the analysis of the current distribution in both ends of a diagonal type MHD generator, it is assumed that the electric quantities, such as the current, electric field etc., vary with x and y (see Fig. 1), and that the gas velocity and temperature depend on only y according to Eq.s (18) and (19) which will be presented later. Also, the gas is assumed to be compressible.

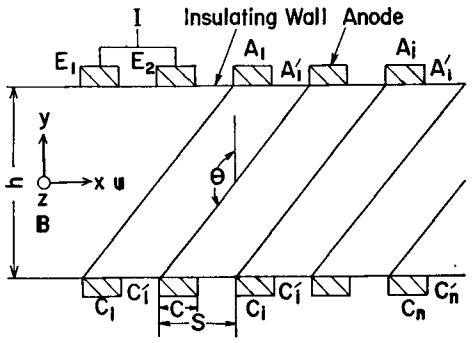

Fig. 1. Coordinate system and generator duct configuration (A type).

As the basic equations for the gas plasma of the MHD duct, we use the following Maxwell's equations

$$\nabla\times\boldsymbol{E}=0,\quad \nabla\cdot\boldsymbol{B}=0,\quad \nabla\cdot\boldsymbol{J}=0\,, \tag{1}$$

and the generalized Ohm's law

$$\boldsymbol{J}=\sigma(\boldsymbol{E}+\boldsymbol{u}\times\boldsymbol{B}+\nabla p_e/en_e)-\beta\boldsymbol{J}\times\boldsymbol{B}/B+\beta\beta_i(\boldsymbol{J}\times\boldsymbol{B})\times\boldsymbol{B}/B^2\,. \tag{2}$$

In these equations

$\boldsymbol{B}$: magnetic flux density vector,

$\boldsymbol{E}$: electric field intensity vector,

e : electron charge,
$\boldsymbol{J}$: current density vector,
$p_e=n_e k T_e$: electron partial pressure,
k : Boltzmann's constant,
n_e : electron density,
T_e : electron temperature,
$\boldsymbol{u}$: gas velocity vector,
β : Hall parameter for electron,
β_i : Hall parameter for ion,
σ : electrical conductivity.

Next we assume $\boldsymbol{E}$, $\boldsymbol{J}$, $\boldsymbol{B}$ and $\boldsymbol{u}$ as follows:

$$\left.\begin{aligned} &\boldsymbol{E}=(E_x, E_y, 0), \quad \boldsymbol{J}=(J_x, J_y, 0)\,, \\ &\boldsymbol{B}=(0, 0, B), \quad\quad \boldsymbol{u}=(u, 0, 0)\,. \end{aligned}\right\} \tag{3}$$

In addition, the secondary magnetic induction induced by $\boldsymbol{J}$ is assumed to be negligible compared with the applied induction, because the magnetic Reynolds number of the gas plasma is much smaller than unity under the operating conditions.

Next, in order to evaluate the current distribution in the generator duct, let us adopt the conventional stream function Ψ defined by

$$J_x=\partial\Psi/\partial y, \quad J_y=-\partial\Psi/\partial x\,. \tag{4}$$

Then, by Eq.s (1) to (4) we can derive the following equation

$$\nabla^2\Psi+P\partial\Psi/\partial x+Q\partial\Psi/\partial y=R\,, \tag{5}$$

where

$$\left.\begin{aligned} P&=(\sigma/\varepsilon)\{\partial(\varepsilon/\sigma)/\partial x-\partial(\beta/\sigma)/\partial y\}\,, \\ Q&=(\sigma/\varepsilon)\{\partial(\varepsilon/\sigma)/\partial y+\partial(\beta/\sigma)/\partial x\}\,, \\ R&=(\sigma/\varepsilon)\{-\partial(\partial p_e/\partial y/en_e)/\partial x+\partial(\partial p_e/\partial x/en_e)/\partial y+u\partial B/\partial x\}\,, \end{aligned}\right\} \tag{6}$$

in which

$$\varepsilon=1+\beta\beta_i\,. \tag{7}$$

2.2 Boundary and subsidiary conditions

First, the boundary condition on the electrode surfaces is

$$E_x=0\,. \tag{8}$$

Next the one on the insulating wall surface is

$$J_y = 0 . \tag{9}$$

Using Eq.s (2) and (4), these conditions (8) and (9) are changed as follows:

$$\varepsilon\partial\Psi/\partial v - \beta\partial\Psi/\partial x - \sigma\partial p_e/\partial x/en_e = 0 , \tag{8}'$$

$$\Psi = \text{const}, \tag{9}'$$

respectively.

Next, in the diagonal type generator, the potential difference must be zero between the anode A_i and cathode C_i which are shorted each other as shown in Fig. 1. Therefore the first subsidiary condition is obtained as follows:

$$V_i = -\int_{A_i}^{C_i} \boldsymbol{E}\cdot d\boldsymbol{s} = 0, \quad i = 1, 2, \cdots, n , \tag{10}$$

where $d\boldsymbol{s}$ is the line element vector of an optional integral path from A_i to C_i and V_i is the potential difference between A_i and C_i.

Next, as the current which runs through an arbitary surface S_i crossing the insulating wall surfaces A_i' and C_i' is equal to the load current I, the second subsidiary condition is obtained as follows:

$$\int_{S_i} \boldsymbol{J}\cdot d\boldsymbol{S} = I, \quad i = 1, 2, \cdots, n , \tag{11}$$

where $d\boldsymbol{S}$ is the element vector of the surface S_i.

Lastly, let us assume that the electric quantities vary periodically in the period of the electrode pitch s along the gas flow behind the n-th electrode pair A_n and C_n. Then the periodicity for the current density $\boldsymbol{J}(x)$ is given as follows:

$$\boldsymbol{J}(x+s) = \boldsymbol{J}(x) . \tag{12}$$

By Eq.s (4), this equation is transformed as follows:

$$\Psi(x+s) = \Psi(x) + I_y^{(n)} , \tag{12}'$$

where $I_y^{(n)}$ is the current flowing into A_n.

The current distributions in the diagonal type generator can be obtained by numerically solving Eq. (5) under the conditions Eq.s (8)′ to (11) and (12)′.

2.3 Calculation of potential

When Eq. (5) is digitally solved under the boundary conditions (8)′ and (9)″ and the subsidiary conditions (10), (11) and (12)′, then with the obtained numerical solution of Ψ, the electric field $\boldsymbol{E}$ at the optional point can be evaluated through Eq.s (2), (3) and (4). Hence, the potential at any point can be cal-

culated by the numerical line integration of $\boldsymbol{E}$ along an arbitary integral path from a reference point to the considered point.

3. Electrical Conductivity, Hall Parameter and Gas Velocity

3.1 Electrical conductivity and Hall parameter

The electrical conductivity σ and the Hall parameter β are given by

$$\sigma = n_e e^2/m_e\nu_e\,, \tag{13}$$

$$\beta = eB/m_e\nu_e = \mu_e B\,, \tag{14}$$

where the electron density n_e is given by the Saha equation

$$\left.\begin{aligned} n_e^2 &= n_s(2\pi m_e kT_e h'^2)^{3/2}\exp(-eV_i'/kT),\\ n_s &= n_{s0}-n_e\,, \end{aligned}\right\} \tag{15}$$

and the average electron momentum transfer collision frequency ν_e by

$$\left.\begin{aligned} \nu_e &= (8kT_e/\pi m_e)^{1/2}(n_sQ_s+n_0Q_0+n_eQ_{ei})\,,\\ &\text{in which}\\ Q_{ei} &= 3.90(e^2/8\pi\varepsilon_0 kT_e)^2\log\Lambda\,,\\ \Lambda &= 12\pi(\varepsilon_0 kT_e/e^2)^{3/2}n_e^{-1/2}\,. \end{aligned}\right\} \tag{16}$$ [6]

In Eq. (13) to (16)

h' : Plancks constant,
m_e : electron mass,
n_0 : parent gas atom density,
n_s : seed atom density,
n_{s0} : seed atom density before ionization,
Q_0 : collision cross-section between electron and parent gas atom,
Q_s : collision cross-section between electron and seed atom,
Q_{ei} : collision cross-section between electron and ion,
V_i' : ionization voltage of seed atom,
ε_0 : dielectric constant of vacuum,
$\mu_e = e/m_e\nu_e$: electron mobility.

Next, the electron temperature T_e is determined by the following electron energy equation

$$3n_e\nu_e m_e\delta k(T_e-T)/2m = J^2/\sigma,\quad J = |\boldsymbol{J}| \tag{17}$$

where

m : mass of parent gas atom,
T : gas temperature,
δ : collision loss factor.

3.2 Gas velocity and temperature distribution

As assumed in Article 2.1, the gas velocity $\boldsymbol{u}$ has only the x component u, and u and T are independent of x, and those vary only in the y direction according to the following relations

$$u/u_0 = \{4y/h \cdot (1-y/h)\}^m \tag{18}$$

and

$$(T-T_W)/(T_0-T_W) = \{4y/h \cdot (1-y/h)\}^{m'} \tag{19}$$

respectively, where

h : duct height,
T_0 : gas temperature at the center of flow, namely $y=h/2$,
T_W: wall temperature,
u_0 : gas velocity at the center of flow.

4. Configuration of Applied Magnetic induction and Arrangement of Output Electrodes

4.1 Configuration of applied magnetic induction

Though generally the intensity of the impressed magnetic induction is a function of the distance along the MHD generator duct, we assume that it is constant in the central domain and decreases linearly in the end regions of the gen-

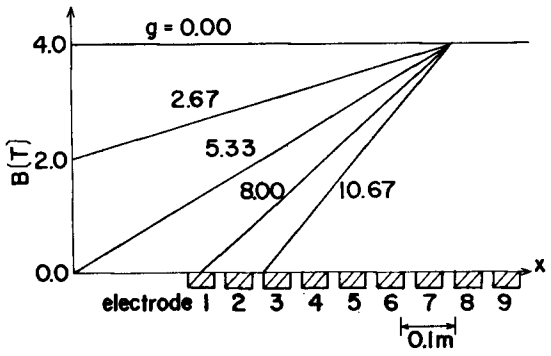

Fig. 2. Configuration of applied magnetic induction.

erator. Also it is assumed that the secondary magnetic induction by the curernt is able to be neglected, since the magnetic Reynolds number of the working gas plasma is much smaller than unity. Further, in our numerical analysis we assume the five configurations of the magnetic induction as plotted in Fig. 2, where g is the gradient of the magnetic induction.

4.2 Arrangement of output electrodes

Among various types of arrangements of the output electrodes which have been proposed for the diagonal type generator, the authors investigate the effects of three types of arrangements, viz. the A type arrangement coupling other electrodes than diagonally connected ones as the output ones, the B type arrangement shorting two pairs of diagonally connected electrodes as the output ones and the C type arrangement coupling two pairs of Hall connected electrodes as the output ones as shown in Figs. 1 and 3.

In addition, the current distribution in the entrance region becomes almost symmetric with the one in the exit region, since the diffusion term in Eq.s (5) and (6) can be usually neglected in the MHD generator. Therefore, if the current distribution in the entrance region is obtained, the current distribution in the exit region can be known by it.

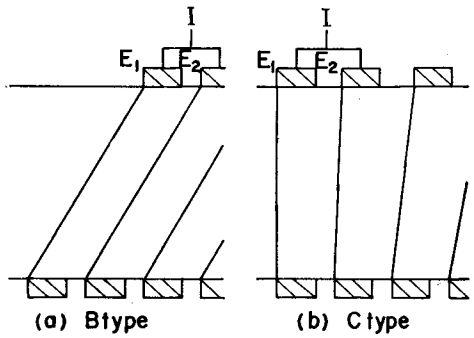

Fig. 3. Generator duct configurations (B and C types).

5. Numerical Methods for Basic Equations

The numerical solution of the current in the MHD generator is sought through the difference analogues of the normalized forms of the basic equations which are introduced in Section 2.

5.1 Normalized basic equations and boundary and subsidiary conditions

Now putting

$$\left.\begin{aligned} &\xi = x/s, \quad \zeta = y/s, \quad \psi = \Psi/(I/w)\,, \\ &T_e' = T_e/T_0, \quad n_e' = n_e/n_0\,, \end{aligned}\right\} \tag{20}$$

where n_0 is the electron density obtained with Eq. (15) in the case of $T_e = T_0$, and w the duct width in z direction, Eq.s (5), (6), (8)′, (9)′, (12)′ and (17) are normalized as follows:

$$\nabla^2\psi + P'\partial\psi/\partial\xi + Q'\partial\psi/\partial\zeta + R' = 0\,, \tag{21}$$

$$\left.\begin{aligned} P' &= (\sigma/\varepsilon)\{\partial(\varepsilon/\sigma)/\partial\xi - \partial(\beta/\sigma)/\partial\zeta\}\,, \\ Q' &= (\sigma/\varepsilon)\{\partial(\beta/\sigma)/\partial\xi + \partial(\varepsilon/\sigma)/\partial\zeta\}\,, \\ R' &= \frac{w}{I}\frac{k}{e}\frac{\sigma}{\varepsilon}\frac{T_0}{n_e'}\left(\frac{\partial T_e'}{\partial\xi}\frac{\partial n_e'}{\partial\zeta} - \frac{\partial T_e'}{\partial\zeta}\frac{\partial n_e'}{\partial\xi}\right) + \frac{w}{I}\frac{\sigma}{\varepsilon}su\frac{\partial B}{\partial\xi}\,, \end{aligned}\right\} \tag{22}$$

$$\frac{\partial\psi}{\partial\zeta} = \frac{\beta}{\varepsilon}\frac{\partial\psi}{\partial\xi} + \frac{k}{e}\frac{\sigma}{\varepsilon}\frac{T_0}{n_e'}\frac{w}{I}\frac{\partial}{\partial\xi}(n_e'T_e')\,, \tag{23}$$

$$\psi = \text{const}, \tag{24}$$

$$\psi(\xi+1, \zeta) = \psi(\xi, \zeta) + I_y^{(n)}/(I/w)\,, \tag{25}$$

$$(3n_0T_0m_e\delta/2m)n_e'\sigma\nu_e(T_e' - T/T_0) = (I/sw)^2\{(\partial\psi/\partial\xi)^2 + (\partial\psi/\partial\zeta)^2\}\,, \tag{26}$$

respectively.

5.2 Basic difference equations

Defining

$$\psi_{ij} = \psi(x_i, y_j), \quad x_i = i\Delta, \quad y_j = j\Delta, \quad i = 1, 2, \cdots, \tag{27}$$

by the central difference analogue Eq.s (21) and (23) are transformed as follows:

$$\left.\begin{aligned} &(1+\Delta P_{ij}'/2)\,\psi_{i+1,j} - 4\psi_{ij} + (1-\Delta Q_{ij}'/2)\,\psi_{i-1,j} \\ &\quad + (1+\Delta Q_{ij}'/2)\,\psi_{i,j+1} + (1-\Delta Q_{ij}'/2)\,\psi_{i,j-1} + \Delta^2 R_{ij}'^2 = 0\,, \\ &i, j = 1, 2, \cdots, \end{aligned}\right\} \tag{21}'$$

$$\left.\begin{aligned} &\psi_{i,j+1} - \psi_{i,j-1} - (\beta/\varepsilon)(\psi_{i+1,j} - \psi_{i-1,j}) \\ &\quad + \{kwT_0\sigma/(eIn_e'\varepsilon)\}(n_{ei+1,j}'T_{ei+1,j}' - n_{ei-1,j}'T_{ei-1,j}') \\ &i, j = 1, 2, \cdots, \end{aligned}\right\} \tag{23}'$$

where P_{ij}', Q_{ij}', R_{ij}', n_{eij}' and T_{eij}' are the values of P', Q', R', n_e' and T_e' at the point (x_i, y_j), respectively. Here $\psi_{i,j-1}|_{j=1}$ and $\psi_{i,j-1}|_{j=h/\Delta'}$, which can't exist physically, can be easily eliminated from Eq.s (21)′ and (23)′ for the electrode surfaces.

In addition, with respect to the authors' numerical example of the MHD generator, it was seen that if the forward or backward difference schemes are applied to the electrode surfaces, it is very difficult to find out the converging solutions of the basic equations.

Finally the simultaneous difference equations (21)′ can be solved under Eq.s (23)′, (24) and (25) by means of the SOR method (successive over-relaxation method). However, for converging the calculation of the strong current concentration which rises often at the electrode edges in the MHD generator, our basic difference equations need a considerably smaller relaxation parameter $\omega=\omega^*$ $(=0.1\sim0.4)$ than unity which is near the conventional value of the parameter. Therefore the digital computation can not rapidly converge and so wastes very much time.

Accordingly the authors adopt the above small value ω^* for ω only in the numerical calculation near the electrodes. On the other hand, they use the other relaxation parameter $\omega=\omega_0$ $(=1\sim2)$ of the conventional magnitude so as to accelerate the calculation within the duct excepting the neighborhood of the electrodes. Moreover, if the residuals of the solutions of the difference equations decrease, the authors increase ω_0 by a suitable one ω', and conversely if they increase, the authors decrease ω_0 by another suitable one ω''.

5.3 Numerical method for subsidiary conditions

In a diagonal generator, the numerical solutions which are obtained by Eq.s (21)′ and (23)′ are required to satisfy the two subsidiary conditions (10) and (11).

First substituting Eq.s (20) in (11), we get the following equations

$$\psi_i^{A'}-\psi_i^{C'}=1, \quad i=1, 2, \cdots, n, \tag{28}$$

where $\psi_i^{A'}$ and $\psi_i^{C'}$ are the values of ψ on the insulating wall surfaces A_i' and C_i'.

If I and $\psi_i^{A'}$'s are given plausible values, the values of $\psi_i^{C'}$'s are decided by Eq. (28). Solving Eq.s (21)′ and (23)′ with these values of I, $\psi_i^{A'}$'s and $\psi_i^{C'}$'s and the appropriately assumed values of σ, β, ε, n_e and T_e, we can obtain the numerical solution of ψ. Next using the solution, we can get the values of E_x and E_y by Eq.s (2), (3) and (4), and further decide the values of V_i by substituting the values of E_x and E_y into the integral $V_i=-\int_{C_i}^{A_i}\boldsymbol{E}\cdot d\boldsymbol{s}$ in Eq.s (10). However the obtained value of V_i is not necessarily equal to zero.

So let us consider the averaged resistance between the electrodes C_i and A_i, namely

$$R_i=h/\{\langle\sigma\rangle_i cw\cos(\pi-\theta)\}, \quad i=1, 2, \cdots, n, \tag{29}$$

where

c : width of electrode,
θ : slope angle between electrode pair,
$\langle\sigma\rangle_i$: mean electrical conductivity of plasma,

and we assume that an imaginary current given by

$$I_i = V_i/R_i, \quad i = 1, 2, \cdots, n \tag{30}$$

flows in the resistance R_i. Then, in order to make V_i zero, it is necessary to flow the opposing current $-I_i$ in R_i. On the other hand, since the normalized current running into the anode A_i is $\psi_{i+1}^{A'}-\psi_i^{A'}$, it is needed to increase $\psi_{i+1}^{A'}-\psi_i^{A'}$ by

$$-I_i/I = -V_i\langle\sigma\rangle_i cw \cos(\pi-\theta)/hI \tag{31}$$

Accordingly beginning with the new modified values of $\psi_i^{A'}$'s, again we must carry out the above mentioned calculation processes. Further, when V_i becomes adequately small after many repetitions of the above mentioned processes, we can obtain the satisfactory numerical solution of ψ.

5.4 Numerical calculation processes

The processes, in which the authors solve numerically the basic difference equations (21)′ under the boundary conditions (23)′ and (24) and the subsidiary conditions (28) and (31), are as follows:

(a) The values of I and $\psi_i^{A'}$s ($i=1, 2, \cdots, n$) are assumed plausibly and the values of $\psi_i^{C'}$s ($i=1, 2, \cdots, n$) are decided to satisfy the subsidiary condition (28).

(b) the reasonable values of σ, β, ε, n_e and T_e are given and then the value of ψ is obtained by solving Eq. (21)″ under Eq.s (23)′, (24) and (25) with the SOR method.

(c) Using the Newton-Raphson method, the value of T_e is derived from Eq. (26), in which is adopted the value of ψ obtained in the previous process (b). Then the values of σ, β, ε and n_e are determined through Eq.s (13) to (16).

(d) The digital computations in the processes (b) and (c) are repeated until ψ converges to a constant value for I, $\psi_i^{A'}$s and $\psi_i^{C'}$s given in (a).

(e) In order to satisfy the subsidiary conditions (10) and (11), here again $\psi_i^{A'}$s and $\psi_i^{C'}$s are given according to Eq.s (28) and (31). After the processes (b), (c) and (d) are repeated, the desirable value of ψ is acquired.

6. Numerical Investigation

6.1 When σ and μ_e are assumed constant

As a numerical example, we analyze the current and potential distributions

in the diagonal type MHD generator duct, in which

$$\left.\begin{aligned} &h = 0.3, \quad s = 0.075, \quad w = 0.3\ [m]\ , \\ &B_0 = 4[\mathrm{T}], \quad I = 150\ [\mathrm{A}], \quad \theta = 153\ [^\circ], \quad n = 9\ , \\ &\sigma = 5.0\ [\mathrm{\mho/m}], \quad \mu_e = 0.5, \quad u_0 = 800\ [\mathrm{m/s}]\ , \end{aligned}\right\} \tag{32}$$

In Fig.s 4 and 5, we plot the current distributions in the duct of the A type arrangement in the case of $g=0$ and 8 [T/m] respectively. From Fig. 4, it is seen that the current concentrates at the edge of only the first output electrode and the second electrode makes little play as the output electrode, when the magnetic induction B does not attenuate. On the other hand, Fig. 5 shows that the nearly equal currents flow into both electrodes, when there exists a suitable attenuation of B. Also Fig. 5 denotes that the current concentration at the edges of output electrodes weakens, since β becomes small in the area suffering a spatial

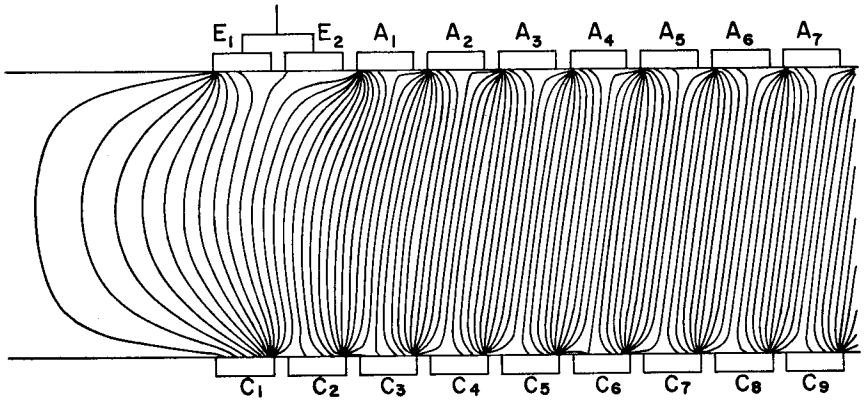

Fig. 4. Current distribution for A type and $g=0.00$.

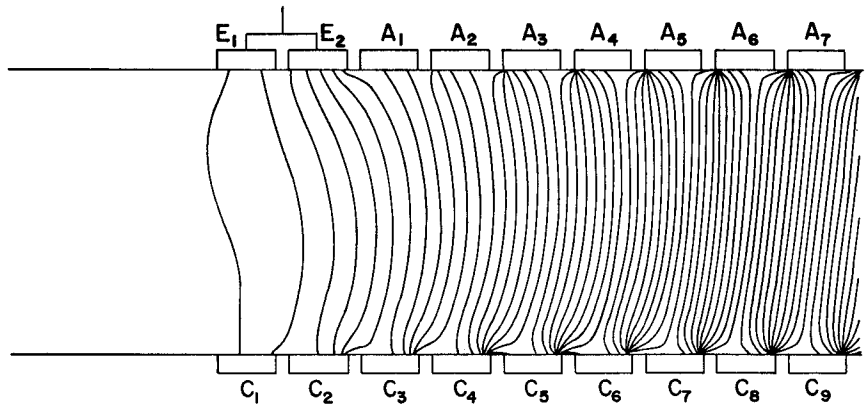

Fig. 5. Current distribution for A type and $g=8.00$.

attenuation of B. Further, both Figs. 4 and 5 show that the eddy currents cease in both cases. Fig. 5 also tells that arranging the output electrodes within the attenuating domain of B does not have an appreciable influence on the current distribution in the central part of generator.

Next, Figs. 6 and 7 show the current distributions in the ducts of the B and C type arrangements respectively in the case of $g=8$. It will be seen that Figs. 6 and 7 give current distributions similar to the one in Fig. 5.

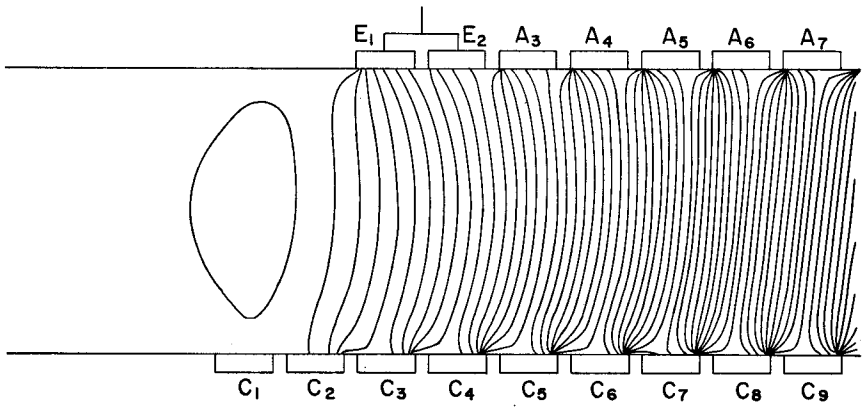

Fig. 6. Current distribution for B type and $g=8.00$.

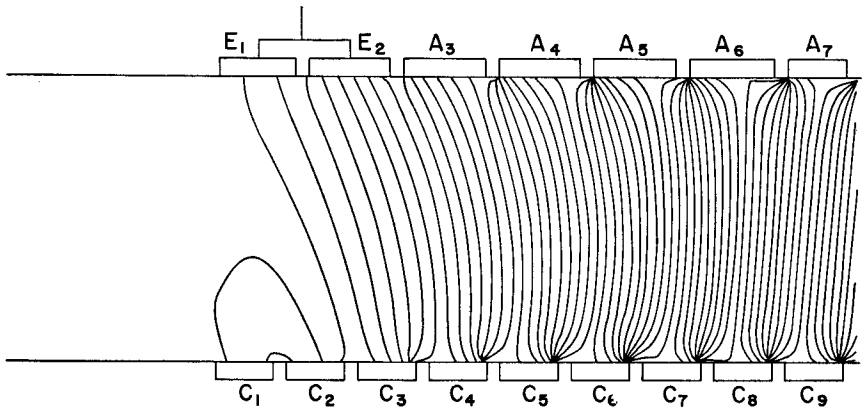

Fig. 7. Current distribution for C type and $g=8.00$.

Next, Fig. 8 shows the potential differences between the electrode pairs A_1-C_1 to A_8-C_8 and the electrode E_1 in the A type arrangement. The figure indicates that the relatively large potential difference arises between the adjacent electrodes when B does not attenuate but that the potential difference becomes smaller as g becomes larger and the potential difference between the adjacent

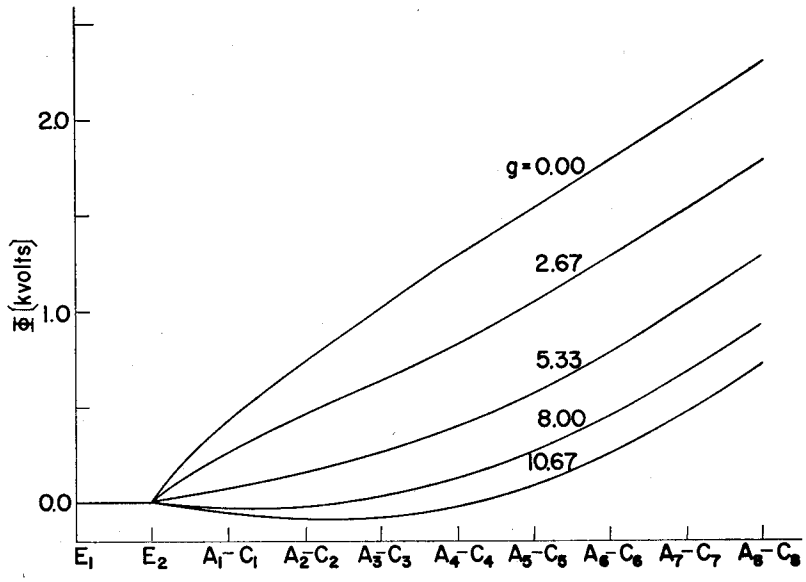

Fig. 8. Distribution of electrode potentials for A type.

electrodes E_2 and A_1 will be almost negligible in the range of $g=5.33$ to 8.00. With respect to both the B and C type arrangements, the similar results are also obtained.

From the above mentioned investigation, we may say that if the output electrodes are set in the area of constant magnetic induction, the potential difference between the adjacent electrodes becomes large, and so large ballast resistors are necessary. On the other hand, if the output electrodes are disposed in the area of a properly attenuating magnetic induction, the above difference is insignificant and large ballast resistors are possibly unnecessary. Further a proper arrangement of the electrodes and a suitable magnetic field distribution can almost suppress occurrences of the eddy current in the generator inlet and otulet.

6.2 When σ and μ_e vary spatially

We investigate the case where σ and μ_e vary spatially in the generator duct according to Eq.s (13) to (17) and

$$\left.\begin{aligned} &h = 0.2, \quad s = 0.1, \quad w = 0.1 \text{ [m]}, \\ &B_0 = 2 \text{ [T]}, \quad I = 70 \text{ [A]}, \quad \theta = 135°, \quad n = 5, \\ &u_0 = 2000 \text{ [m/s]}, \quad \delta = 2, \\ &T_0 = 1800, \quad T_W = 1600 \text{ [K]}. \end{aligned}\right\} \tag{33}$$

In Fig. 9, the current distribution in the A type duct in the case of $g=5.33$ is plotted. The figure tells that the current distribution in the case of variable

σ and μ_e is fairly more complicated than that in the case of constant σ and μ_e. However, the potential distribution in the case of variable σ and μ_e is very similar to that in Fig. 8. Therefore, most of the results introduced in the previous article are qualitatively proper to the present case.

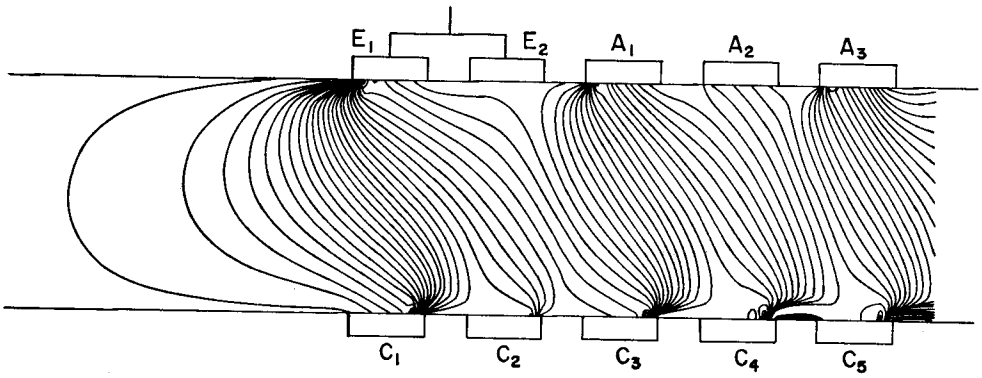

Fig. 9. Dependence of current distribution on spatial variation of σ and μ_e.

7. Conclusions

The main conclusions derived from the above mentioned numerical analysis are as follows:

(1) When the output electrodes are disposed in the region with a suitably decreasing magnetic induction, the potential differences between the adjacent electrodes become very small and large ballast resistors are needless.

(2) Proper arrangement of the output electrodes and appropriate distribution suitable of magnetic induction can almost extinguish the eddy current.

(3) Disposing output electrodes within the attenuating area of magnetic induction has little influence on the current distribution in the central part of the generator.

(4) The variety of arrangements of output electrodes has little effect on the current distribution in the generator. Therefore, the type of output electrode disposition is thought to be decided by facility and advantage in manufacturing.

Acknowledgements

The authors wish to express their thanks to Mr. J. Shimada for his help in the numerical calculations, and also to the other members in their laboratory for their kindly advice.

References

1) H. Hurwitz et al.: J. Appl. Phys., 32, No. 2, 205–216 (1961).
2) L. Dzung: Brown Boveri Review, 49, No. 6, 211–225 (1962).
3) W. Norris et al.: Pro. I.E.E., 115, 555–561 (1968).
4) J. Houben et al.: AIAA, 10, No. 11, 1513–1516 (1972).
5) M. Ishikawa, J. Shimada and J. Umoto: Convention Records at the Annual Meeting of I.E.E.J., No. 173 (1976).
6) T. Noguchi: A thesis for a doctor's degree, p. 27 (1970).
7) L. Lengyel: Energy Con., 9, 13–23 (1969).

Appendix

Relaxation Parameter in SOR Method

In general, simultaneous linear equations are written in the following matrix form

$$A\boldsymbol{x} = \boldsymbol{b}, \quad A = D-E-F, \tag{App. 1}$$

where

A : square matrix,
$\boldsymbol{b}$: known column vector,
D : diagonal matrix,
E : lower triangular matrix,
F : upper triangular matrix,
$\boldsymbol{x}$: unknown column vector.

Now let us consider the following relaxation parameter matrix

$$\Omega = \begin{pmatrix} \omega_1 & 0 & \cdots & 0 \\ 0 & \omega_2 & \ddots & \vdots \\ \vdots & \ddots & \ddots & \vdots \\ 0 & \cdots & 0 & \omega_m \end{pmatrix}, \tag{App. 2}$$

where ω_i ($i=1, 2, \cdots, m$; m: total node number) is the relaxation parameter for the i-th node, then the $k+1$-th approximation $\boldsymbol{x}^{(k+1)}$ for $\boldsymbol{x}$ is given by

$$\boldsymbol{x}^{(k+1)} = \boldsymbol{x}^{(k)}+\Omega\{D^{-1}(\boldsymbol{b}+E\boldsymbol{x}^{(k+1)}+F\boldsymbol{x}^{(k)})-\boldsymbol{x}^{(k)}\} . \tag{App. 3}$$

Further, this equation is rewritten as follows:

$$\left.\begin{aligned} \boldsymbol{x}^{(k+1)} &= M\boldsymbol{x}^{(k)}+\boldsymbol{g} \\ &= M^k\boldsymbol{x}^{(1)}+(M^{(k-1)}+\cdots+M+U)\boldsymbol{g} \end{aligned}\right\} \tag{App. 4}$$

where

$$\left.\begin{aligned} &U \ : \text{unit matrix,} \\ &M = (U-\Omega D^{-1}\boldsymbol{E})^{-1}\{I+\Omega(D^{-1}F-U)\}\ , \\ &\boldsymbol{g} \ = (U-\Omega D^{-1}E)^{-1}\Omega D^{-1}\boldsymbol{b}\ . \end{aligned}\right\} \qquad \text{(App. 5)}$$

Next, if $\lim_{k\to\infty} ||M|| < 1$, where $||M||$ is the norm of M,

$$\lim_{k\to\infty} \boldsymbol{x}^{(k-1)} = (U-M)^{-1}\boldsymbol{g} = A^{-1}\boldsymbol{b}\ . \qquad \text{(App. 6)}$$

Namely, when k tends to ∞, the value of $\boldsymbol{x}^{(k+1)}$ converges to the solution of Eq. (App. 1).

Moreover,if A is a symmetric positive matrix, it can be proved that $\boldsymbol{x}$ converges for $0<\omega_i$ $(i=1, 2, \cdots, m)<2$.